Acta Cryst B
STRUCTURAL SCIENCE
CRYSTAL ENGINEERING
MATERIALS
ISSN 2052-5206

Co-crystals of an organic triselenocyanate with ditopic Lewis bases: recurrent chalcogen bond interactions motifs

Asia Marie S. Riel,[a,b] Olivier Jeannin,[a] Orion B. Berryman[b] and Marc Fourmigué[a]*

[a]ISCR (Institut de Sciences Chimiques de Rennes), Universite Rennes, CNRS, UMR 6226, 35000 Rennes, France, and [b]Department of Chemistry and Biochemistry, University of Montana, 32 Campus Dr., Missoula, MT 59812, USA. *Correspondence e-mail: marc.fourmigue@univ-rennes1.fr

Received 22 October 2018
Accepted 15 December 2018

Edited by A. Nangia, CSIR–National Chemical Laboratory, India

Keywords: chalcogen bond; sigma-hole interactions.

Supporting information: this article has supporting information at journals.iucr.org/b

Organic selenocyanates *R*–Se–CN can act as an amphoteric chalcogen bond (ChB) donor (through the Se atom) and acceptor (through the N atom lone pair). Co-crystallization of tri-substituted 1,3,5-tris(selenocyanatomethyl)-2,4,6-trimethylbenzene (1) is investigated with different ditopic Lewis bases acting as chalcogen bond (ChB) acceptors to investigate the outcome of the competition, as ChB acceptor, between the nitrogen lone pair of the SeCN group and other Lewis bases involving pyridinyl or carbonyl functions. In the presence of tetramethylpyrazine (TMP), benzoquinone (BQ) and *para*-dinitrobenzene (*p*DNB) as ditopic Lewis bases, a recurrent oligomeric motif stabilized by six ChB interactions is observed, involving six SeCN groups and the ChB acceptor sites of TMP, BQ and *p*DNB in the 2:1 adducts $(1)_2$·TMP, $(1)_2$·BQ and $(1)_2$·*p*DNB.

1. Introduction

Following extensive investigations on halogen bonding interactions as a rediscovered tool in crystal engineering (Cavallo *et al.*, 2016; Gilday *et al.*, 2015), recent approaches have highlighted the generality of the σ-hole concept (Cavallo *et al.*, 2014) and its extension to chalcogen (S, Se, Te), pnictogen (P, As, Sb) and tetrel (Si, Ge, Sn) elements. Halogen atoms are well known to develop one single σ-hole in the prolongation of the C—X bond, allowing for an unprecedented predictability in crystal engineering strategies. The situation is rather different with chalcogens since the presence of two covalent bonds leads to the appearance of two σ-holes (Wang *et al.*, 2009; Alkorta *et al.*, 2018; Bleiholder *et al.*, 2006); as theoretically analyzed in model compounds (Politzer *et al.*, 2017; Pascoe *et al.*, 2017; Bauzá & Frontera, 2018), and experimentally illustrated in the crystal structures of $Se(CN)_2$ (Klapötke *et al.*, 2004; Klapötke *et al.*, 2008), selenophthalic anhydride (Brezgunova *et al.*, 2013) and tellurophene derivatives (Benz *et al.*, 2016; Sánchez-Sanz & Trujillo, 2018). Similar to halogen bonding, chalcogen bond donors are also investigated as Lewis acids in catalysis (Wonner *et al.*, 2017; Benz *et al.*, 2018). We recently postulated that the unsymmetrical substitution of the chalcogen atom, for example in organic selenocyanates *R*—Se—CN could strongly favor one σ-hole over the other. We found indeed that crystal structures of organic selenocyanates exhibit a recurrent supramolecular motif where the Se atom interacts with the lone pair on the N atom of a neighboring SeCN moiety (Jeannin *et al.*, 2018), leading to the formation of extended chains ···Se(*R*)CN···Se(*R*)CN···, most probably stabilized by

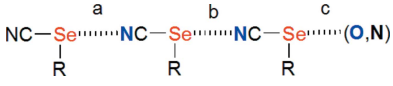

cooperativity. The formation of these motifs is hindered when the selenocyanate is faced with stronger Lewis bases (such as 4,4′-bipyridine) and the Se atoms then interact with the pyridinic nitrogen atom, with an even shorter Se···N distance (Huynh *et al.*, 2017). Intermolecular (Maartmann-Moe *et al.*, 1984) as well as intramolecular (Wang *et al.*, 2018) Se···O_2N– interactions can also displace the nitrogen atom of the SeCN moiety from interaction with a neighboring Se atom.

In the course of our investigations of the solid-state arrangement of benzylic selenocyanates, we turned our attention to tri-substituted derivatives such as 1,3,5-tris-(selenocyanatomethyl)-2,4,6-trimethylbenzene (1). It was found to crystallize either alone or as a solvate with DMF or AcOEt (Jeannin *et al.*, 2018). In the three structures, we confirmed the formation of recurrent linear ChB motifs where the lone pair of the nitrogen atom in the *R*—Se—CN moiety interacts as Lewis base with the σ-hole located on the Se atom, essentially in the prolongation of the NC–Se bond. As shown in Fig. 1(*a*) for the DMF solvate, *i.e.* (1)·DMF, this interaction pattern was complemented with a side interaction between the Se atom and the oxygen atom of DMF. On the other hand, in the AcOEt solvate [Fig. 1(*b*)], the carbonyl oxygen atom displaces one nitrogen atom of a SeCN group to enter into a strong Se···O=C(OEt)Me interaction (Jeannin *et al.*, 2018). A question then arises about the outcome of the ChB competition of a given Se atom as a ChB donor, when interacting either with the N atom of a neighboring SeCN moiety or with another Lewis base. We report here on the outcome of the co-crystallization of (1) with three different ditopic Lewis bases, namely tetramethylpyrazine (TMP), benzoquinone (BQ) and *para*-dinitrobenzene (*p*DNB), allowing us to evaluate the robustness of these one-dimensional ···Se(*R*)CN···Se(*R*)CN··· motifs.

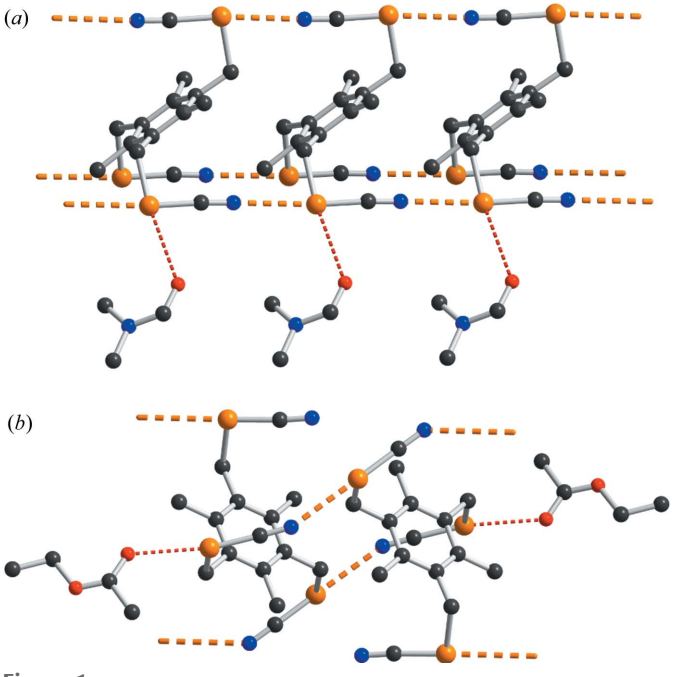

Figure 1
Details of the ChB interactions (orange thick dotted lines for the Se···N interactions, red thin dotted lines for the Se···O interactions) in the solvates of (1) with: (*a*) DMF, (*b*) AcOEt. Hydrogen atoms were omitted for clarity. Only one of the two disordered AcOEt molecules in (*b*) is shown.

2. Experimental

2.1. Crystal growth

Compound (1) was prepared as described by Jeannin *et al.* (2018). All cocrystals were obtained from vapor diffusion of diethyl ether into ethyl acetate (2 ml) mixtures of two equivalents of (1) (10.7 mg, 11 mg and 10.8 mg, respectively)

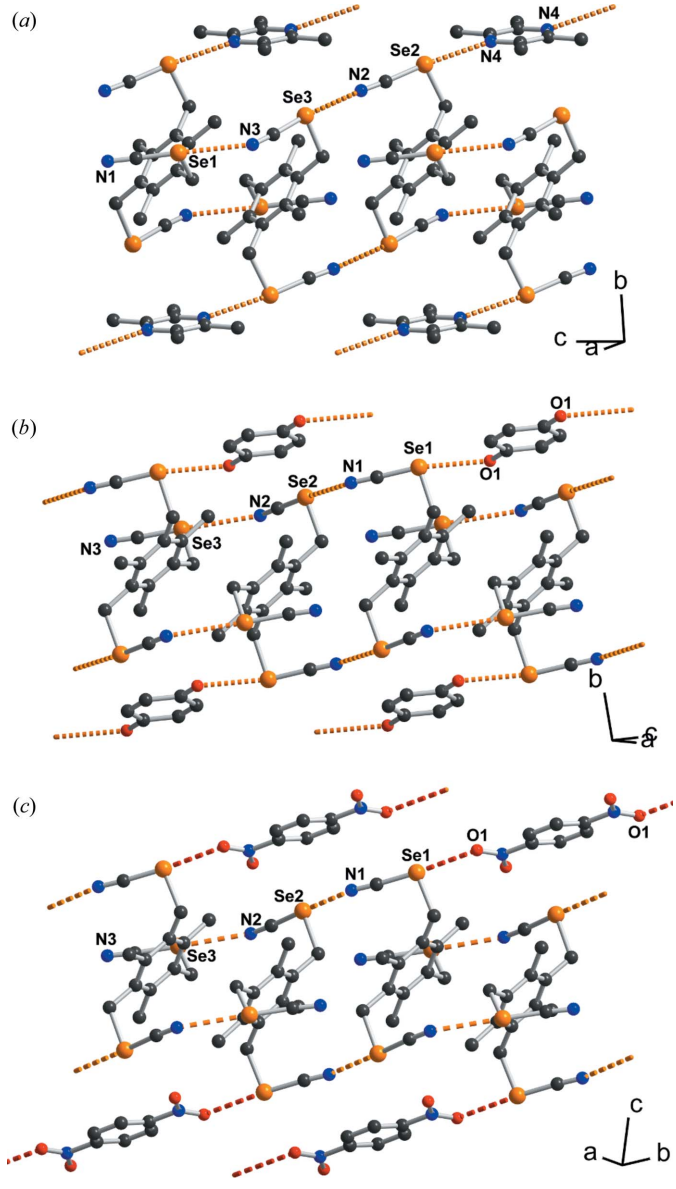

Figure 2
Views of the ChB interactions in: (*a*) $(1)_2$·TMP, (*b*) $(1)_2$·BQ and (*c*) $(1)_2$·*p*DNB. Hydrogen atoms have been omitted for clarity. The ChB interactions are indicated as orange (Se···N) or red (Se···O) dotted lines.

Table 1
Experimental details.

For each structure determination: T = 296 (2) K, triclinic, space group $P\bar{1}$, Z = 2, Bruker-AXS APEXII diffractometer, multi-scan absorption correction (*SADABS*; Krause *et al.*, 2015), H-atom parameters constrained.

	(1)·0.5TMP	(1)·0.5BQ	(1)·0.5*p*DNB
Crystal data			
Chemical formula	$C_{15}H_{15}N_3Se_3·0.5(C_8H_{12}N_2)$	$C_{15}H_{15}N_3Se_3·0.5(C_6H_4O_2)$	$C_{15}H_{15}N_3Se_3·0.5(C_6H_4N_2O_4)$
M_r	542.28	528.23	558.23
a, b, c (Å)	9.797 (3), 10.560 (3), 10.656 (3)	10.008 (2), 10.4345 (19), 10.760 (2)	10.187 (3), 10.415 (2), 11.232 (3)
α, β, γ (°)	87.528 (10), 69.844 (8), 87.528 (9)	93.538 (5), 117.528 (5), 95.282 (5)	75.891 (8), 82.213 (9), 61.753 (8)
V (Å^3)	1033.5 (5)	985.3 (3)	1017.8 (5)
μ (mm^{-1})	5.35	5.61	5.44
Crystal size (mm)	0.13 × 0.04 × 0.02	0.28 × 0.02 × 0.01	0.31 × 0.03 × 0.01
Data collection			
T_{min}, T_{max}	0.774, 0.899	0.874, 0.945	0.822, 0.947
No. of measured, independent and observed [$I > 2\sigma(I)$] reflections	25 685, 4706, 2995	24 136, 4486, 2412	16 919, 4665, 2903
R_{int}	0.057	0.088	0.050
(sin $\theta/\lambda)_{max}$ (Å^{-1})	0.648	0.650	0.650
Refinement			
$R[F^2 > 2\sigma(F^2)]$, $wR(F^2)$, S	0.041, 0.092, 1.00	0.054, 0.140, 1.00	0.042, 0.106, 0.97
No. of reflections	4706	4486	4665
No. of parameters	240	229	247
$\Delta\rho_{max}$, $\Delta\rho_{min}$ (e Å^{-3})	0.70, −0.53	0.82, −0.66	1.10, −0.47

Computer programs: *APEX2* (Bruker, 2014), *SIR92* (Altomare *et al.*, 1994), *SHELXL*2014/7 (Sheldrick, 2014), *ORTEP* for Windows (Farrugia, 2012), *WinGX* publication routines (Farrugia, 2012).

and one equivalent of either TMP (2.2 mg), BQ (3.5 mg) or *p*DNB (2.8 mg).

2.2. Crystallography

Single-crystal X-ray diffraction data were collected at room temperature on an APEXII Bruker-AXS diffractometer operating with graphite-monochromated Mo $K\alpha$ radiation (λ = 0.71073 Å). The structures were solved by direct methods using the *SIR92* (Altomare *et al.*, 1994) program and then refined with full-matrix least-square methods based on F^2 (*SHELXL*-2014/7; Sheldrick, 2015) with the aid of the *WINGX* (Farrugia, 2012) program. All non-hydrogen atoms were refined with anisotropic atomic displacement parameters. H atoms were finally included in their calculated positions. Crystallographic data on X-ray data collection and structure refinements are given in Table 1.

3. Results and discussion

Co-crystallization of (1) with either TMP, BQ or *p*DNB was performed by mixing solutions of both partners in ethyl acetate and diffusing the mixture with diethyl ether. Crystals formed after two days. All three co-crystals crystallize in the triclinic system, space group $P\bar{1}$, with the tris(selenocyanate) derivative (1) in the general position in the unit cell, and the ditopic ChB acceptor on the inversion center; hence the 2:1 stoichiometry, that is $(1)_2$·TMP, $(1)_2$·BQ and $(1)_2$·*p*DNB. The three structures are closely related (Fig. 2). Among the three independent SeCN groups in (1), two are engaged in an Se···NC ChB while the third one is engaged in a ChB with the oxygen or nitrogen atom of the coformer, TMP, BQ or *p*DNB. It gives rise locally to the recurring of inversion-centered oligomeric ChB motifs shown in Fig. 3.

A comparison of the ChB characteristics within the three compounds (see Table 2 and Scheme 1) shows a large dispersion of the Se···NC ChB distances, from 2.96 to 3.31 Å, that is a reduction ratio (RR) relative to the sum of the van der Waals radii (1.90 + 1.55 = 3.45 Å) in the range 0.86–0.96. The Se···O ChB contacts are slightly shorter, with RR down to 0.86, in line with the smaller van der Waals radius of O (1.52 Å) versus N (1.55 Å).

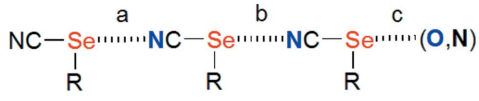

Scheme 1

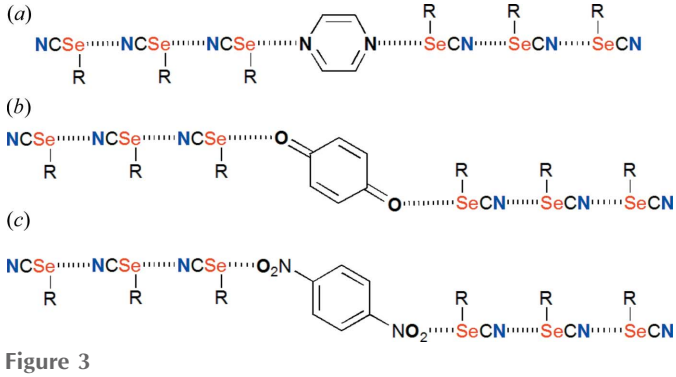

Figure 3
Schematic representation of the oligomeric chalcogen-bonded motifs found in: (*a*) $(1)_2$·TMP, (*b*) $(1)_2$·BQ and (*c*) $(1)_2$·*p*DNB.

Table 2
ChB characteristics.

Refer to Scheme 1 for positions of the ChB.

	ChB a		ChB b		ChB c		
	Se···N (Å)	C—Se···N (°)	Se···N (Å)	C—Se···N (°)	Se···N,O (Å)	C—Se···N,O (°)	Reference
TMP	3.096 (6)	178.8 (2)	3.029 (11)	175.0 (2)	3.171 (11) (N)	172.6 (2) (N)	This work
BQ	3.315 (15)	177.1 (3)	3.192 (10)	174.6 (3)	2.966 (13) (O)	170.7 (3) (O)	This work
*p*DNB	3.063 (20)	178.8 (2)	2.989 (9)	175.3 (2)	3.231 (11) (O)	161.9 (2) (O)	This work
AcOEt	3.174 (4)	177.0 (1)	2.965 (3)	174.9 (1)	2.925 (6)† (O) 2.871 (3)† (O)	166.5 (2) (O) 168.8 (2) (O)	Jeannin *et al.* (2018)

† The oxygen atom of the carbonyl group in AcOEt is disordered on two equiprobable positions.

The closely related structural motifs found in $(1)_2$·TMP, $(1)_2$·BQ and $(1)_2$·*p*DNB, are also found in their solid-state organization in the crystal. As shown in Fig. 4, we note the recurrent formation of stacks of (1), interconnected through the Se···(O, N) ChB interaction with TMP, BQ or *p*DNB molecules acting as ditopic ChB acceptors between the chains.

The efficiency of benzylic selenocyanates such as (1) to act as strong ChB donors can be traced back from the amplitude of the σ-hole generated on the selenium atom. As shown in Fig. 5, the electrostatic surface potential (ESP) map calculated with an extremum surface potential V_s (see Politzer *et al.*, 2017) for (1) shows the presence of positively charged areas in the prolongation of the three C—Se bonds, with $V_{s,max}$ of 41.1 kcal mol^{-1}. This value can be compared with that calculated for the model benzylselenocyanate $PhCH_2$–SeCN molecule where it amounts to 36.4 kcal mol^{-1}, or with that calculated for the reference halogen bond donor F_5C_6–I (35.7 kcal mol^{-1}) under the same conditions. These calculations demonstrate that tri-substitution actually activates the three individual ChB donor moieties.

These similarities also demonstrate that the three ChB acceptors used here can play a very similar role as ditopic Lewis bases. An interesting analogy can be made with halogen bonding (XB) if we compare reported structures involving these three molecules (TMP, BQ, *p*DNB) and a common XB donor such as 1,4-diiodoperfluorobenzene. Indeed, *p*-$I_2F_4C_6$ has been reported to co-crystallize with TMP (CSD refcode JAQMAQ; Syssa-Magalé *et al.*, 2005) and BQ (CSD refcode ZARFUV; Liu *et al.*, 2012), while the non-fluorinated 1,4-diiodobenzene has been co-crystallized with *p*DNB (CSD refcode YESZEB; Allen *et al.*, 1994). As shown in Fig. 6, the three reported structures show a recurrent 1D structure where TMP, BQ and *p*DNB also play a similar role.

In conclusion, we have shown here that specific supramolecular motifs can be obtained from the ChB interaction of the *tri*-substituted derivative (1) with three different ditopic Lewis bases: TMP, BQ and *p*DNB. The sizeable ChB interactions with the nitro group in DNB allow us to infer that benzylic selenocyanate derivatives such as (1) could be used for the detection of nitrated molecules of interest for their

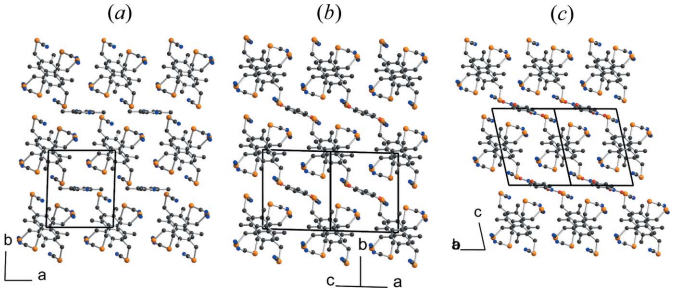

Figure 4
Solid state organization in (*a*) $(1)_2$·TMP viewed in projection along *c* axis, (*b*) $(1)_2$·BQ viewed in projection along *ac* and (*c*) $(1)_2$·*p*DNB viewed in projection along *ab*.

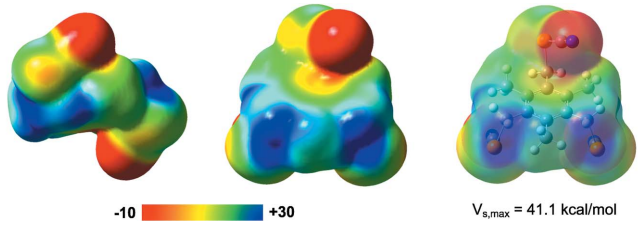

Figure 5
Three views of the computed electrostatic surface potential of (1) (0.001 a.u. molecular surface). Potential scale ranges from −10 kcal mol^{-1} to 30 kcal mol^{-1}. From DFT calculations with B3LYP functional, 6-31+G** basis set for C, H and N, LANDL2Ddp ECP basis set for Se.

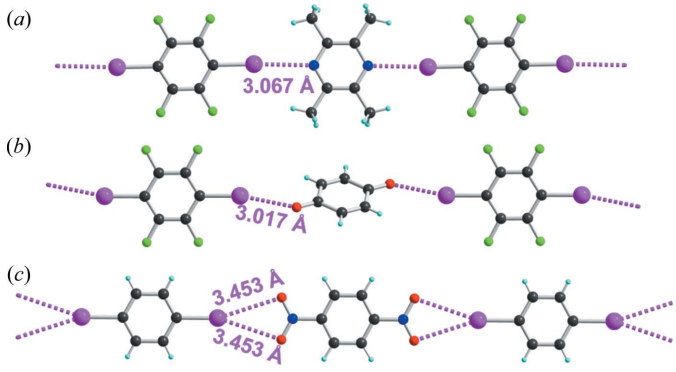

Figure 6
Detail of the one-dimensional structures stabilized by 1,4-diiodoperfluorobenzene XB with the three ditopic molecules (*a*) TMP, (*b*) BQ and (*c*) *p*DNB, acting as analogous XB acceptors.

energetic properties, such as TNT (trinitrotoluene) or HNS (hexanitrostilbene) (Schubert & Kuznetsov, 2012; Caygill *et al.*, 2012).

Funding information

The following funding is acknowledged: Agence Nationale de la Recherche (grant No. ANR-17-CE07-0025-02 to Marc Fourmigué); Rennes Metropole (bursary No. A17.612 to Asia Marie S. Riel); French Embassy in Washington (Chateaubriand Fellowship) (award to Asia Marie S. Riel); National Science Foundation (grant No. CAREER CHE-1555324).

References

Alkorta, I., Elguero, J. & Del Bene, J. E. (2018). *ChemPhysChem*, **19**, 1756–1765.

Allen, F. H., Goud, B. S., Hoy, V. J., Howard, J. A. K. & Desiraju, G. R. (1994). *J. Chem. Soc. Chem. Commun.* pp. 2729–2730.

Altomare, A., Cascarano, G., Giacovazzo, C., Guagliardi, A., Burla, M. C., Polidori, G. & Camalli, M. (1994). *J. Appl. Cryst.* **27**, 435–436.

Bauzá, A. & Frontera, A. (2018). *Molecules*, **23**, 699.

Benz, S., Macchione, M., Verolet, Q., Mareda, J., Sakai, N. & Matile, S. (2016). *J. Am. Chem. Soc.* **138**, 9093–9096.

Benz, S., Poblador-Bahamonde, A. I., Low-Ders, N. & Matile, S. (2018). *Angew. Chem. Int. Ed.* **57**, 5408–5412.

Bleiholder, C., Werz, D. B., Köppel, H. & Gleiter, R. (2006). *J. Am. Chem. Soc.* **128**, 2666–2674.

Brezgunova, M., Lieffrig, J., Aubert, E., Dahaoui, S., Fertey, P., Lebègue, S., Ángyán, J., Fourmigué, M. & Espinosa, E. (2013). *Cryst. Growth Des.* **13**, 3283–3289.

Bruker (2014). *APEX2*. Bruker AXS Inc., Madison, Wisconsin, USA.

Cavallo, G., Metrangolo, P., Milani, R., Pilati, T., Priimagi, A., Resnati, G. & Terraneo, G. (2016). *Chem. Rev.* **116**, 2478–2601.

Cavallo, G., Metrangolo, P., Pilati, T., Resnati, G. & Terraneo, G. (2014). *Cryst. Growth Des.* **14**, 2697–2702.

Caygill, J. S., Davis, F. & Higson, S. P. J. (2012). *Talanta*, **88**, 14–29.

Farrugia, L. J. (2012). *J. Appl. Cryst.* **45**, 849–854.

Gilday, L. C., Robinson, S. W., Barendt, T. A., Langton, M. J., Mullaney, B. R. & Beer, P. D. (2015). *Chem. Rev.* **115**, 7118–7195.

Huynh, H.-T., Jeannin, O. & Fourmigué, M. (2017). *Chem. Commun.* **53**, 8467–8469.

Jeannin, O., Huynh, H.-T., Riel, A. M. S. & Fourmigué, M. (2018). *New J. Chem.* **42**, 10502–10509.

Klapötke, T. M., Krumm, B., Gálvez-Ruiz, J., Nöth, H. & Schwab, I. (2004). *Eur. J. Inorg. Chem.* pp. 4764–4769.

Klapötke, T. M., Krumm, B. & Scherr, M. (2008). *Inorg. Chem.* **47**, 7025–7028.

Krause, L., Herbst-Irmer, R., Sheldrick, G. M. & Stalke, D. (2015). *J. Appl. Cryst.* **48**, 3–10.

Liu, P., Ruan, C., Li, T. & Ji, B. (2012). *Acta Cryst.* E**68**, o1431.

Maartmann-Moe, K., Sanderud, K. A. & Songstad, J. (1984). *Acta Chem. Scand.* **38**, 187–200.

Pascoe, D. J., Ling, K. B. & Cockroft, S. L. (2017). *J. Am. Chem. Soc.* **139**, 15160–15167.

Politzer, P., Murray, J. S., Clark, T. & Resnati, G. (2017). *Phys. Chem. Chem. Phys.* **19**, 32166–32178.

Sánchez-Sanz, G. & Trujillo, C. (2018). *J. Phys. Chem. A*, **122**, 1369–1377.

Schubert, H. & Kuznetsov, A. (2012). Editors. *Detection of Bulk Explosives: Advanced Techniques against Terrorism.* NATO ARW Proceedings, Springer.

Sheldrick, G. M. (2015). *Acta Cryst.* C**71**, 3–8.

Syssa-Magalé, J.-L., Boubekeur, K., Palvadeau, P., Meerschaut, A. & Schöllhorn, B. (2005). *CrystEngComm*, **7**, 302–308.

Wang, H., Liu, J. & Wang, W. (2018). *Phys. Chem. Chem. Phys.* **20**, 5227–5234.

Wang, W., Ji, B. & Zhang, Y. (2009). *J. Phys. Chem. A*, **113**, 8132–8135.

Wonner, P., Vogel, L., Kniep, F. & Huber, S. M. (2017). *Chem. Eur. J.* **23**, 16972–16975.